CONVEX ANALYSIS AND SEPARATION OF COMPOSITE SIGNALS IN DCE-MRI

Li Chen[1], Tsung-Han Chan[2,1], Peter L Choyke[3], Chong-Yung Chi[2], Ge Wang[1], Yue Wang[1]

[1]Dept of Electrical and Computer Eng, Virginia Polytechnic Institute and State University, Arlington, VA, USA
[2]Institute Communications Eng and Dept of Electrical Eng, National Tsing Hua University, Hsinchu, Taiwan
[3]Molecular Imaging Program, National Cancer Institute, National Institutes of Health, Bethesda, MD, USA

ABSTRACT

Dynamic functional imaging promises powerful tools for the visualization and elucidation of important disease-causing biological processes, where the pixels often represent a composite of multiple biomarkers independent of spatial resolution. This study exploits both blind source separation and imagery marker characteristics to develop a hybrid method for the separation of mixed yet correlated biomarker distributions in DCE-MRI. A compartment latent variable model is constructed upon which a novel convex analysis framework is proposed to provide a close-form algebraic solution to separating composite markers with non-negativity and well-grounded points. A unique non-negative clustered component analysis is further developed to explicitly consider both partial volume effect and noise contamination. Experimental results show promising and robust extraction of time activity curves and vascular marker images in agreement with biomedical expectations.

Index Terms—Blind source separation, compartment model, convex analysis, tumor angiogenesis, dynamic contrast-enhanced magnetic resonance imaging

1. INTRODUCTION

Dynamic imaging exploits the joint-effect of probe-target interactions and promises simultaneous imaging of multiple biomarkers, where the pixel values often represent a composite of distinct sources independent of spatial resolution. Dynamic contrast-enhanced magnetic resonance imaging (DCE-MRI) uses various molecular weight contrast agents to assess tumor vascular permeability and quantify cellular and molecular abnormalities in blood vessel walls [1, 2]. Specifically, tumor tissue is made up of sub-regions with heterogeneous kinetics, so the signal of pixels often reflects multiple microenvironments in a tumor, thus represents a complex summation of vascular permeability with various perfusion rates [2]. Recent research aims to simultaneously dissect the spatial-temporal characteristics of source signals (permeability of different perfusions).

Various methods have been proposed for separating the composite biomarker signals in dynamic functional imaging. The major limitations associated with the existing methods include unrealistic assumptions of the computational model (such as source independence and model identifiability) [3],

inability of acquiring in vivo temporal/spectral characteristic curves of the probes [4], and vulnerability to noise impact [5]. This motivates the consideration of a hybrid blind source separation approach that exploits both the temporal diversity of probe dynamics and the non-negativity of the biomarker images. A convex analysis based algebraic solution, coupled with scatter plot clustering, is proposed to extract the angiogenic permeability distributions (APD) and time activity curves (TAC) from dynamically mixed DCE-MRI image sequences.

2. THEORY AND METHOD

2.1 Compartment model

We introduce a compartment latent variable model of DCE-MRI. We adopt a two-tissue compartment model to illustrate the spatial-temporal probe kinetics, where the tumor activities consist of fast and slow turnover pools, see Fig. 1.

Specifically, we use a latent variable model to describe the relationship between APD and TAC, as well as the plasma input. Let $\mathbf{x}(i) = [x(i,t_1), x(i,t_2),...,x(i,t_L)]^T$ be the observed tissue activities at pixel i measured over L time points, i.e., the time activity curve of pixel i. Now consider the APD $\mathbf{k}(i) = [k_f(i), k_s(i), k_p(i)]^T$ together with a $L \times 3$ mixing matrix $\mathbf{A}$ which maps the latent space to the data space via $\mathbf{x}(i) = \mathbf{Ak}(i)$:

$$\begin{bmatrix} x(i,t_1) \\ x(i,t_2) \\ \vdots \\ x(i,t_L) \end{bmatrix} = \begin{bmatrix} a_f(t_1) & a_s(t_1) & a_p(t_1) \\ a_f(t_2) & a_s(t_2) & a_p(t_2) \\ \vdots & \vdots & \vdots \\ a_f(t_L) & a_s(t_L) & a_p(t_L) \end{bmatrix} \begin{bmatrix} k_f(i) \\ k_s(i) \\ k_p(i) \end{bmatrix}, \quad (1)$$

where subscripts f, s, p represent the fast flow, slow flow and input function respectively, N is the number of pixels and

$$\begin{aligned} a_f(t) &= c_p(t) \otimes e^{-k_{2f}t}, \\ a_s(t) &= c_p(t) \otimes e^{-k_{2s}t}, \quad (2) \\ a_p(t) &= c_p(t), \end{aligned}$$

where $\otimes$ denotes convolution operation; $c_p(t)$ is the tracer concentration in plasma (the input function); k_{2f} and k_{2s} are the rate constants for efflux in the fast flow and slow

flow pools respectively [6]; we define compartment TACs as $\mathbf{a}_j = [a_j(t_1), a_j(t_2),...,a_j(t_L)]$, $j = f,s,p$, associated with the corresponding APDs. Fig.1 (b) illustrates the patterns of $a_f(t)$, $a_s(t)$, $a_p(t)$. It can be seen that the observation $\mathbf{x}(i)$ is linear combination of $\mathbf{a}_j$, $j \in \{f,s,p\}$, weighted by $k_f(i)$, $k_s(i)$, and $k_p(i)$.
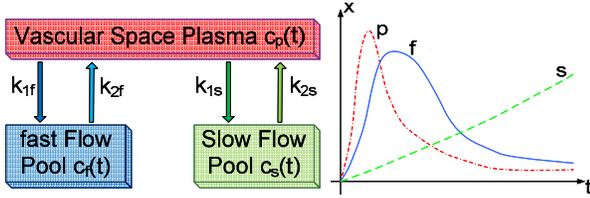
Fig. 1 Two-tissue compartment model and time-activity curves of perfusions for quantifying tumor vascular characteristics based on DCE-MRI. The patterns of interests include the heterogeneous spatial distribution of vascular permeability associated with fast and slow diffusions. (a) Schematic diagram. (b) Supposed time activity curve of fast flow, slow flow, and input function, denoted by f, s, p respectively.

Since $\mathbf{k}(i)$ and $\mathbf{A}$ are both unknown, the reconstruction of the model can be formulated as a blind source separation (BSS) problem, where the task is to find an unmixing matrix $\mathbf{W}$ from $\mathbf{x}(i)$ such that

$$\hat{\mathbf{k}}(i) = \mathbf{Wx}(i) = \mathbf{WAk}(i) = \mathbf{Pk}(i) \qquad (3)$$

where $\hat{\mathbf{k}}(i)$ is the estimated $\mathbf{k}(i)$ up to a permutation $\mathbf{P}$.

2.2 Well Grounded Points

As aforementioned, the compartment model given by (1) can be alternatively expressed as

$$\mathbf{x}(i) = \sum_j^{f,s,p} \mathbf{a}_j k_j(i), \qquad (4)$$

where $k_j(i) \geq 0$ and $\mathbf{a}_j$ for $j \in \{f,s,p\}$ are linearly independent vectors due to the heterogeneous property. Based on the realistic tumor characteristics in DCE-MRI that the vasculatures of different compartments have their own unique perfusion patterns, we assume that there exists a point index $i_{WGP,j}$ such that $\mathbf{k}(i_{WGP,j})$ satisfies

$$\mathbf{k}(i_{WGP,j}) = k_j(i_{WGP,j})\mathbf{e}_j, \quad j \in \{f,s,p\},$$

where $k_j(i_{WGP,j}) > 0$ and $\mathbf{e}_j$ is the jth standard base. This kind of points $\mathbf{k}(i_{WGP,j}), j \in \{f,s,p\}$ is referred herein to *well grounded points (WGPs)* and the corresponding observations $\mathbf{x}(i_{WGP,j})$ are called as extreme points. Therefore $\mathbf{x}(i_{WGP,j})$ has the same dynamic patterns as the corresponding compartment TAC, i.e.,

$$\mathbf{x}(i_{WGP,j}) = k_j(i_{WGP,j})\mathbf{a}_j, \quad j \in \{f,s,p\}. \qquad (5)$$

For the verification of WGPs assumption, we employ soft clustering methods such as expectation maximization (EM) and fuzzy C means method to cluster $\mathbf{x}(i)$ of DCE-MRI

data. We discovered that most pixels have unique membership to a single cluster with negligible associations with other clusters, and the cluster centers shows similar dynamic patterns as fast flow and slow flow compartment TACs. This fact supports the assumption of WGPs.

2.3 Convexity Pyramid Method

We exploit some concepts of convex geometry to analyze the latent variable compartment model, which is not only suitable for (4) but also for the case of any number of sources, denoted by K. A *convex pyramid* of a set of vectors $A = \{\mathbf{a}_j \in \mathbb{R}^L, j = 1,2,...,K\}$ is the set of all the non-negative combinations of $\mathbf{a}_1,...,\mathbf{a}_K$, defined as

$$\mathbb{P}_{\text{convex}}\{A\} = \left\{\sum_{j=1}^K \alpha_j \mathbf{a}_j \mid \mathbf{a}_j \in A, \ \alpha_j \geq 0\right\}.$$

where vectors $\mathbf{a}_1,...,\mathbf{a}_K$ are the lateral edges of $A = \{\mathbf{a}_1,...,\mathbf{a}_K\}$ if A is linearly independent.

Lemma 1 (Convex geometry of observation scatter plot). *Suppose* $X = \{\mathbf{x}(i), i = 1,...,N\}$, $\mathbf{x}(i) = \sum_{j=1}^K k_j(i)\mathbf{a}_j$, *the source components* $k_j(i) \geq 0$ *and* $\mathbf{A} = [\mathbf{a}_1,...,\mathbf{a}_K]$ *is a full-rank real-valued matrix, then* $X = \{\mathbf{x}(1),\cdots,\mathbf{x}(N)\}$ *is confined within a convex pyramid of* A, *i.e.,* $X \subseteq \mathbb{P}_{\text{convex}}\{A\}$.

Lemma 1 suggests that all the observations X are enclosed by a convex pyramid whose lateral edges are $\mathbf{a}_1,...,\mathbf{a}_K$. With the existence of WGPs, albeit shall be possible to obtain the information about $\mathbf{a}_1,...,\mathbf{a}_K$ from the set of observations X, as described in the following Theorem 1.

Theorem 1 (Identifiability). *Suppose that the source components* $k_j(i) \geq 0$ *and there is at least one WGP on each of the K coordinate axes,* $\mathbf{x}(i) = \sum_{j=1}^K k_j(i)\mathbf{a}_j$ *and* $\mathbf{A} = [\mathbf{a}_1,...,\mathbf{a}_K]$ *is a full-rank real-valued matrix, then the lateral edges of* $\mathbb{P}_{\text{convex}}\{X\}$ *are* $\mathbf{a}_1,...,\mathbf{a}_K$.

Theorem 1 suggests immediately the possibility of identifying the mixing matrix $\mathbf{A}$ by determining the lateral edges of $\mathbb{P}_{\text{convex}}\{X\}$, i.e. $\mathbf{x}(i_{\text{WGP},j}), j = 1,...K$. A geometric illustration of Theorem 1 for $K = 3$ is shown in Fig. 2. The blue dots are the observations $\mathbf{x}(1),\cdots,\mathbf{x}(N)$ forming the convex pyramid $\mathbb{P}_{\text{convex}}\{X\}$. The red dots circled by broken line are the observations on the three lateral edges of the convex pyramid, i.e.

1558

$$\mathbf{x}\left(i_{WGP,j}\right) = k_j\left(i_{WGP,j}\right)\mathbf{a}_j, \quad j=1,2,3 ,$$

which also represents the column vectors of $\mathbf{A}$ except for a componential scaling by WGPs.
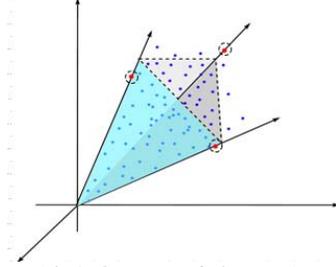
Fig.2: Geometry of Theorem 1.

To utilize some existing extreme point search methods for a convex hull, we perform a normalization procedure over time that maps all the observations $\mathbf{x}(1),\cdots,\mathbf{x}(N)$ onto a hyperplane so that the normalized observations $\overline{\mathbf{x}}(1),\cdots,\overline{\mathbf{x}}(N)$ satisfy

$$\sum_{l=1}^{L}\overline{x}_l(i) = 1 , \tag{6}$$

where $\overline{x}_l(i)$ is the lth component of the normalized data points.

The problem for identifying the lateral edges of a convex pyramid suggested by Theorem 1 is then converted into the search of the extreme points of a convex hull, stated in the following lemma.

Lemma 2 (Normalization & Convex Hull). *Suppose there is at least one WGP on each of the K coordinate axes in source space and* $\mathbf{A}$ *is a full-rank real-valued mixing matrix, then the convex pyramid of* $\overline{\mathbf{x}}(1),\cdots,\overline{\mathbf{x}}(N)$ *becomes a convex hull whose extreme points are the normalized lateral edges (or the normalized column vectors of mixing matrix).*

This problem for determining the extreme points of a convex hull can be solved by the readily available quickhull algorithm. Note that we omit all the proofs of Lemma 1, Theorem1, and Lemma 2 due to space limit, and their detailed proofs will be given in our up coming journal paper.

From convex pyramid algorithm and (5), ideally pixel TACs $\mathbf{x}(i)$ in DCE-MRI data will form a convex pyramid whose edges have the same directions as $\mathbf{a}_f, \mathbf{a}_s, \mathbf{a}_p$, and the corresponding $\mathbf{k}(i)$ are well grounded points.

The proposed convex pyramid method was tested on simulated dual-energy chest x-ray images. Figs. 3(a) and 3(b) correspond to the source images of soft tissue and bony structures. We apply the convex pyramid method to the simulated linear combination of the source images and recover them as shown in Figs. 3(d) and 3(e). Fig. 3(c) is the scatter plot of 3(a) and 3(b) while 3(f) is the scatter plot of 3(d) and 3(e), where the estimated source images and their scatter plot resemble quite well the ground truth.
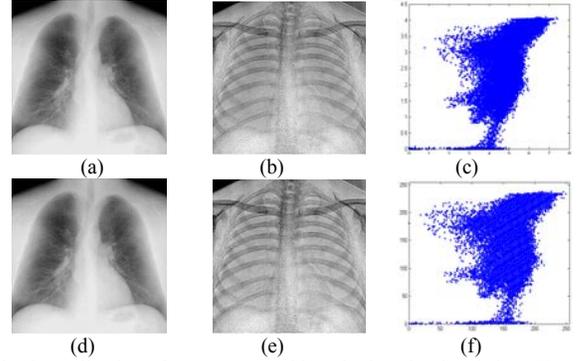
Fig. 3 Application of convex pyramid method to simulated chest X-ray.

2.4 Non-negative Clustered Component Analysis

However, the real DCE-MRI data may be affected by heavy noise and partial volume effect (PVE) [7], thus exploring the application of convex pyramid method to DCE-MRI in practice is the subject of ensuing developments.

Our recently proposed non-negative clustered component analysis (nCCA) [8] is designed to remove noise effect. nCCA consists of multivariate soft clustering, information visualization, and spatial aided PVE removal. It works on a Gaussian Mixture Model (GMM) of pure-volume pixels

$$\mathbf{x}_n(i) = \mathbf{a}_j + \boldsymbol{\varepsilon}(i) , \quad j \in \{f,s,p\}, \tag{9}$$

where $\mathbf{x}_n(i)$ is the noisy observation and $\boldsymbol{\varepsilon}(i)$ is assumed to be a zero-mean noise vector with a spatially Gaussian distribution. By employing EM algorithm to cluster $\mathbf{x}_n(i)$, the centers of the Gaussian kernel (the estimated compartment TACs $\mathbf{a}_f, \mathbf{a}_s, \mathbf{a}_p$) can be obtained. With this step, the noisy effect is firstly removed.

2.5 Convexity Measure

Once the original pixels are replaced by the cluster centers estimated by nCCA and defined as $X_c = \{\mathbf{c}_1,\cdots,\mathbf{c}_P\} \subset \mathbb{R}^L$, Our next effort is to apply the convex pyramid method to X_c, so as to obtain vertices of convex hull as $\mathbf{a}_f, \mathbf{a}_s, \mathbf{a}_p$. However, due to some residual error and PVE, selecting a perfect convex hull with assumed three vertices, which must enclose all cluster centers, is unrealistic. Hence, we propose here a convexity measure to obtain an optimum convex hull of 3 well-grounded points among $\mathbf{c}_1,\cdots,\mathbf{c}_P$. The *convexity measure* (CM) is of minimum-margin manner, given by

$$CM = \min_{l_1,\cdots,l_3} \sum_{i=1}^{P} e_i\left(l_1,l_2,l_3\right), \tag{8}$$

where

1559

$$e_i\left(l_1, l_2, l_3\right) = \min_{\theta_1, \theta_2, \theta_3} \left\| \mathbf{c}_i - \sum_{j=1}^3 \theta_j \mathbf{c}_{l_j} \right\|_2^2, \qquad (9)$$

subject to $\sum_{j=1}^3 \theta_j = 1, \theta_j \geq 0 \ \forall j = 1, 2, 3,$ in which $\{l_1, l_2, l_3\} \subset \{1, \cdots, P\}$ and $l_i \neq l_j$ for $i \neq j$. The purpose of the convexity measure is to find a 3-edge convex hull which has minimum sum of margin between the convex hull and points outside it. The inner optimization problem given by (9) is a convex optimization, while the outer optimization problem in (8) could be solved by exhaustive search of C_3^P combinatorial possibilities, since P is reasonably small.

After finding the estimated TACs $\hat{\mathbf{a}}_f, \hat{\mathbf{a}}_s, \hat{\mathbf{a}}_p$, which are the three clustered centers with minimum CM, we can obtain APDs by least-square fitting under non-negative constraint of APD. Specifically, the problem can be formulated as

$$\mathbf{k}(i) = \arg\min_{\mathbf{k}(i)} \left(\| \mathbf{x}(i) - [\mathbf{a}_f, \mathbf{a}_s, \mathbf{a}_p] \cdot \mathbf{k}(i) \|_2 \right)$$
$$\text{s.t.} \quad k_j(i) \geq 0 \ for \ j \in \{f, s, p\} \qquad (10)$$

By (10), we can obtain the estimated APDs $\mathbf{k}(i) = [k_f(i), k_s(i), k_p(i)]^T$.

3. EXPERIMENTAL RESULTS

In this section, we demonstrate the efficacy of our method on the real DCE-MRI data. The data was acquired at NIH Clinical Center using gadolinium DTPA as the contrast agent. Three dimensional DCE-MRI scans were performed every 30 seconds for a total of 11 minutes after the injection of the contrast agent.

We performed several preprocessing steps on the raw data to assure accurate performance. First, we mask part of the image to highlight the region of interest, i.e, tumor site. Second, we eliminate the first and last few images for a meaningful separation because the insignificant tracer uptake on these head/tail images would affect the separation performance. The resultant number of images is then 20.

Figure 4 shows the compartment TACs obtained by the traditional BSS algorithms such as NMF [9] and nICA [3], and by our method. 4(a) and 4(b) show that NMF and nICA fail to obtain the expected compartment TACs where some unexpected patterns, i.e., the slow flow has an apparent down trend at first several time points, violating the biomedical facts that all compartment TACs shall go up initially. The TACs estimated by our proposed framework are shown in 4(c). This result presents a good agreement with biomedical expectation and illustrates the validity of the compartment model given by (1) and (2). Figure 5 shows the reconstructed APD obtained by our method.

4. CONCLUSION

A convexity-principled hybrid method is proposed in this paper, to dissect multiple biomarkers from dynamic functional imaging data. Experimental results coincide with underlying biomedical expectations. Our preliminary studies provide useful theory and information on the utility of the proposed methods for simultaneous imaging of multiple functional or molecular biomarkers. Given the difficulty of the task, while the optimality of these methods may be data or modality dependent, we would expect them to be important tools in dynamic image formation and analysis.
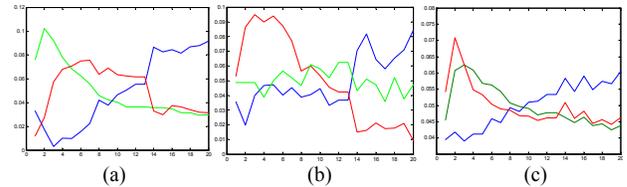
Fig. 4. Compartment TACs obtained by (a) NMF, (b) nICA, and (c) our proposed hybrid method
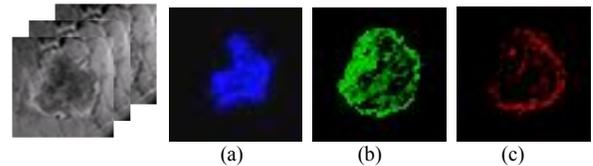
Fig.5. Angiogenic permeability distributions estimated by our proposed framework: (a) slow flow, (b) fast flow, (c) input function.

REFERENCES

[1] D. M. McDonald and P. L. Choyke, "Imaging of angiogenesis: from microscope to clinic," *Nat Med*, vol. 9, pp. 713-725, 2003.

[2] A. R. Padhani and J. E. Husband, "Dynamic contrast-enhanced MRI studies in oncology with an emphasis on quantification, validation and human studies," *Clin Radiol* (56): 607-620, 2001.

[3] E. Oja and M. Plumbley, "Blind separation of positive sources by globally convergent gradient search", Neural Computation, vol. 16, pp. 1811-1825, 2004.

[4] M. Zhao, M. Yang, X.-M. Li, P. Jiang, E. Baranov, S. Li, M. Xu, S. Penman, and R. M. Hoffman, "Tumor-targeting bacterial therapy with amino acid auxotrophs of GFP-expressing Salmonella typhimurium," Proc Natl Acad Sci, vol. 102, pp. 755-760, 2005.

[5] F-Y Wang, et al, "Blind separation of multichannel biomedical image patterns by non-negative least-correlated component analysis," Lecture Notes Bioinfo 4146: 151-162, 2006.

[6] Y. Zhou, et al., "A modelling-based factor extraction for determining spatial heterogeneity of Ga-68 EDTA kinetics in brain tumors," *IEEE Trans. Nucl. Sci.*, vol. 44, pp. 2522-2527, 1997.

[7] P. Santago and H. D. Gage, "Statistical models of partial volume effect," IEEE Trans. Image Processing, vol. 4, pp. 1531-1540, Nov. 1995.

[8] Li Chen, et al, "Separating Composite Signals in Multi-probe Dynamic Imaging", Proc. 41st Annual Asilomar Conference on Signals, Systems, and Computers, Pacific Grove, CA, Nov. 2007.

[9] Daniel D. Lee and H. Sebastian Seung, "Learning the parts of objects by non-negative matrix factorization", Nature, vol. 401 (6755), pp. 788–791, 1999.